nanomaterials

MDPI

Article

Synthesis of $NiCo_2O_4$ Nanostructures and Their Electrochemial Properties for Glucose Detection

Kyu-bong Jang [1,†], Kyoung Ryeol Park [2,†], Kang Min Kim [3,†], Soong-keun Hyun [1], Jae-eun Jeon [2], Young Sik Song [4], Soo-keun Park [4], Kyoung-il Moon [4], Chisung Ahn [4], Sung-chul Lim [4], Jaewoong Lee [4], Jong Cheol Kim [5,*], HyukSu Han [6,*] and Sungwook Mhin [7,*]

1 School of Materials Science and Engineering, Inha University, 25 Younghyun-Dong, Incheon 22201, Korea; jkb0418@kitech.re.kr (K.-b.J.); skhyun@inha.ac.kr (S.-k.H.)
2 Department of Materials Science and Engineering, Hanyang University, 222 Wangsimni-ro, Seoul 04763, Korea; nebula9938@kitech.re.kr (K.R.P.); jaeeun00@kitech.re.kr (J.-e.J.)
3 Korea Institute of Industrial Technology, 137-41 Gwahakdanji-ro, Gangneung 25440, Korea; kmkim@kitech.re.kr
4 Korea Institute of Industrial Technology, 156 Gaetbeol-ro, Incheon 21999, Korea; yssong@kitech.re.kr (Y.S.S.); pskeun@kitech.re.kr (S.-k.P.); kimoon@kitech.re.kr (K.-i.M.); cahn@kitech.re.kr (C.A.); lsc2001@kitech.re.kr (S.-c.L.); woong428@kitech.re.kr (J.L.)
5 Daegu Mechatronics & Materials Institute, Seongseogongdan-r0 11-gil, Dalseo-gu, Daegu 42714, Korea
6 Department of Energy Engineering, Konkuk University, 120 Neungdong-ro, Seoul 05029, Korea
7 Department of Advanced Materials Engineering, Kyonggi University, 154-42 Gwanggyosan-ro, Suwon 16227, Korea
* Correspondence: jckim@dmi.re.kr (J.C.K.); hhan@konkuk.ac.kr (H.H.); swmhin@kgu.ac.kr (S.M.)
† These authors contributed equally to this work.

Abstract: In this work, we prepared spinel-type $NiCo_2O_4$ (NCO) nanopowders as a low-cost and sensitive electrochemical sensor for nonenzymatic glucose detection. A facile and simple chemical bath method to synthesize the NCO nanopowders is demonstrated. The effect of pH and annealing temperature on the formation mechanism of NCO nanoparticles was systematically investigated. Our studies show that different pHs of the precursor solution during synthesis result in different intermediate phases and relating chemical reactions for the formation of NCO nanoparticles. Different morphologies of the NCO depending on pHs are also discussed based on the mechanism of growth. Electrochemical performance of the prepared NCO was characterized towards glucose, which reveals that sensitivity and selectivity of the NCO are significantly related with the final microstructure combined with constituent species with multiple oxidation states in the spinel structure.

Keywords: nickel cobaltite; enzyme-free; glucose sensor

Citation: Jang, K.-b.; Park, K.R.; Kim, K.M.; Hyun, S.-k.; Jeon, J.-e.; Song, Y.S.; Park, S.-k.; Moon, K.-i.; Ahn, C.; Lim, S.-c.; et al. Synthesis of $NiCo_2O_4$ Nanostructures and Their Electrochemial Properties for Glucose Detection. *Nanomaterials* **2021**, *11*, 55. https://doi.org/10.3390/nano11010055

Received: 30 November 2020
Accepted: 24 December 2020
Published: 28 December 2020

1. Introduction

Diabetes is a disease that impairs the human body's ability to control glucose or sugar in the blood [1–3]. High glucose levels can cause serious health problems including heart disease, stroke, and kidney disease, and thus, it is important to maintain the glucose levels in blood via continuous monitoring with accurate detection of glucose [4–6]. Since the oxygen electrode was developed, different types of glucose sensors including an optical sensor and electrochemical sensor have been introduced [7,8]. Especially, the electrochemical glucose sensor has been actively studied to increase the sensitivity and to reduce the detection time for its excellent applicability to the real-time monitoring system.

Electrochemical glucose sensors can be divided into enzymatic and nonenzymatic sensors. The enzymatic glucose sensor exhibits high sensitivity and selectivity through direct immobilization of glucose oxidase. However, its natural limitations include a short lifetime due to poor chemical and thermal stability, and expensive processing costs hindering further advancement of the enzymatic biosensor for industrial applications [9–11]. Thanks

to their several advantages such as long-term stability and reproducibility, and effective processing cost, different types of nonenzymatic electrocatalysts have been developed including noble metals, transition metals and alloys, and metal oxides [12–14]. Among them, transition-metal-based oxides have drawn great interest due to their configurational flexibility of transition metals, which promotes glucose oxidation with excellent sensitivity and selectivity [15–18].

Different types of synthesis methods for transition-metal-based oxides have been developed including hydroxide decomposition [19], nanocasting [20], electrodeposition [21], coprecipitation [22], and hydrothermal synthesis [23]. However, their complex and energy-consuming processing hinders the industrial application to glucose sensors. Therefore, exploring fast, environmentally friendly, and energy-efficient synthetic methods for transition-metal-based oxides is urgent. Recently, it has been reported that chemical bath synthesis has proven to be capable of controlling the size and morphology of materials by control of reaction parameters, such as temperature, pH, and solvent concentration [23–26]. It is expected that the transition-metal-based oxides prepared by chemical bath synthesis can be applied as a glucose sensor. However, there is limited information available on the effect of the processing parameters of chemical bath synthesis on the electrochemical performance for glucose detection.

In this work, spinel-type $NiCo_2O_4$ (NCO) are successfully synthesized by a simple and facile chemical bath method. The morphology of the NCOs depending on pH during synthesis was investigated, which is closely related to the growth mechanism. Also, the formation of the NCOs was investigated to show excellent electrochemical performance for glucose detection including sensitivity, selectivity, and low detection limits.

2. Materials and Methods

2.1. Materials and Reagents

Nickel nitrate hexahydrate ($Ni(NO_3)_2 \cdot 6H_2O$, 99.99%), cobalt nitrate hexahydrate $Co(NO_3)_2 \cdot 6H_2O$, 99.9%), ammonia solution (NH_4OH), sodium hydroxide (NaOH), D-(+)-glucose, uric acid (UA), dopamine (DA), L-ascorbic acid (LA), and acetic acid (AA) were purchased from Sigma-Aldrich (Seoul, Korea). All of the reagents used were of analytical grade and used as received without further purification.

2.2. Chemical Bath Synthesis of NiCo-Layered Double Hydroxide and $NiCo_2O_4$

An aqueous solution of $Ni(NO_3)_2 \cdot 6H_2O$ (0.005 M) and $Co(NO_3)_2 \cdot 6H_2O$ (0.01 M) was prepared by dissolving the salts in 100 mL of deionized water (DI water) with vigorous stirring for 60 min. Ammonia solution was added to the precursor solution until each scheduled pH value (11, 12, 13, and 14) was reached, followed by heating at 80 °C on a hotplate for 14 h, resulting in a thick, viscous, dark greenish fluid. It is noted that the pH of the precursor solution without the addition of ammonia solution was 8. Obtained products prepared at pH 8, 11, 12, 13, 14 are denoted as NCO8B, NCO11B, NCO12B, NCO13B, and NCO14B, respectively. The fluid was filtered through filter paper several times with DI water and ethanol. Subsequently, the filtered materials were dried in air for 24 h followed by annealing in air for 4 h at different temperatures at 450 °C with a heating rate of 10 °C/min, which turned the material black in color. Final products prepared at pH 8, 11, 12, 13, 14 are denoted as NCO8, NCO11, NCO12, NCO13, and NCO14, respectively. Also, crystalline $NiCo_2O_4$ with spinel structure is abbreviated as NCO. For clarity, detailed information is presented in Table S1 in the Supporting Information.

2.3. Material Characterizations and Electrochemical Measurements

The morphologies of NCO were investigated by scanning electron microscopy (SEM, Nova NanoSEM 450, FEI, Portland, OR, USA). The X-ray diffraction (XRD) patterns were collected using a PANalytical X-ray diffractometer (Empyrean, PANanalytical, Almelo, Nederland) with Cu-Kα radiation (λ = 0.1548 nm).

All the electrochemical measurements including cyclic voltammetry (CV) and chronoamperometry (CA) were performed on an IVIUMSTAT electrochemical analyzer (IVIUMSTAT, Ivium Technologies, Eindhoven, Netherland) using a three-electrode system in a 0.1 M aqueous NaOH solution at room temperature. A glassy carbon electrode (GCE), an Ag/AgCl electrode, and a platinum plate were used as the working electrode, reference electrode, and counter electrode, respectively. The samples (10 mg), ethanol (0.5 mL), and Nafion solution (30 µL) were mixed for the preparation of the working electrode. Subsequently, drop-casting of the dispersion on the GC electrode was performed followed by drying under ambient conditions overnight.

The CV response was recorded between 0 and 0.6 V at different scanning rates of 5–100 mV/s. To get the optimal potential of the CA response of the sample, glucose was added to the 0.1 M NaOH solution at various potentials from +0.4 to +0.6 V, as shown in Figure S1. The optimal potential of +0.5 V was chosen, which was highly responsive and stable as the working potential for glucose detection. The CA response of the samples to the glucose was carried out at an applied potential of 0.5 V under stirred conditions. For sensing performance evaluation, 0.01–6 mM glucose solutions were used, with LA, DA, AA, and UA detection performed at concentrations of 0.1 mM in 0.1 M NaOH alkaline electrolyte.

3. Results

The influence of pH during synthesis on the crystallization of the NCO was investigated as shown in Figure 1. As shown in Figure 1a, $Ni_2(NO_3)_2(OH)_2 \cdot 2H_2O$ and $Co(NO_3)_2 \cdot 6H_2O$ were observed from NCO8B, while NiCo-layered double hydroxide (NiCo-LDH) was observed from NCO11B to 14B [27]. As annealing temperature increased, different phase transformations were observed depending on pH as shown in Figure 1b, c. Phase transformation of the NCO8B to spinel-type NCO (NCO8) occurred from 150 °C, and NCO single phase with improved crystallinity was observed at 350 °C, which implies the chemical reaction of the intermediates ($Ni_3(NO_3)_2(OH)_4$ and $Co(NO_3)_2 \cdot 6H_2O$) with oxygen for the formation of spinel-type NCO8. However, NCO11B–14B with LDH structure directly transformed into spinel-type NCOs (NCO11—14) without any chemical reaction between intermediates with increasing temperature. Regardless of pH during synthesis, spinel-type NCO single phase was observed after annealing at 450 °C (Figure 1d) [28]. In the chemical bath process, an increase of OH^- ions in a precursor solution containing Ni^{2+}, $Co^{2+,}$ and $NO_3{}^-$ occurred by applying NH_4OH, which turned into an alkaline condition (pH = 11~14) in the chemical bath. Under the condition, the chemical reaction among different ions such as Ni^{2+}, Co^{2+}, and OH^- ions led to the formation of the NiCo-LDH as expressed by reaction (1) [29,30]. Simultaneously, H_2O molecules and NO^{3-} ions were intercalated into NiCo-LDH interlayer to retain the LDH structure through a hydrogen bond. Subsequent annealing of the as-synthesized NiCo-LDH caused structural transformation into spinel-type $NiCo_2O_4$ (NCO), as described by the reaction (2) [29–32].

$$Ni^{2+} + 2Co^{2+} + 6OH^- \rightarrow NiCo_2(OH)_6 \text{ (NiCo-LDH)} \quad (1)$$

$$2NiCo_2(OH)_6 + O_2 \rightarrow 2NiCo_2O_4 + 6H_2O \quad (2)$$

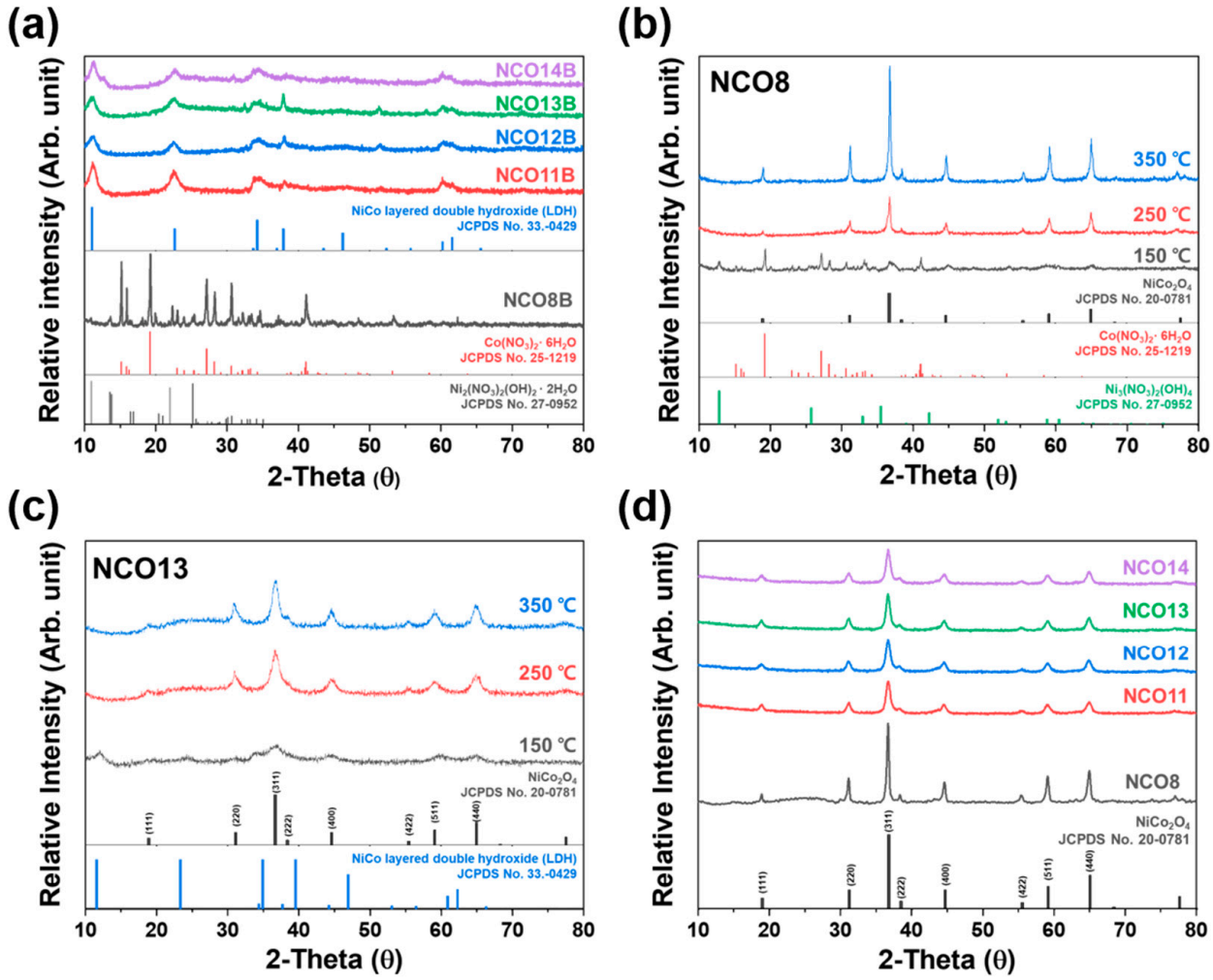

Figure 1. XRD patterns of (**a**) NCOBs (8B, 11B, 12B, 13B, and 14B), (**b**) NCO8 by different annealing temperatures (150, 250, and 350 °C), (**c**) NCO13 by different annealing temperatures (150, 250, and 350 °C), and (**d**) NCOs (8, 11, 12, 13, and 14) after annealing at 450 °C.

The pH depending on OH^- ions in the precursor solution also determines the morphology of the NCO during synthesis. As depicted in Figure 2a, a high concentration of OH^- ions for the reaction environment reveals the flower-like morphology as observed from NCO11B–13B, which is originated from anisotropic grain growth of LDH. [33,34] However, the unique flower-like morphology disappears at pH 14 (NCO14B) due to further grain growth of LDHs. After annealing, the morphological transformation of the NCOB prepared at different pH values was observed as shown in Figure 2b. Spherical nanoparticles were observed from NCO8, derived by the chemical reaction between nitrates and oxygen. However, the transformation from NiCo-LDH prepared at high pH (NCO11–13) to NCO maintains the sheet-like morphology. It is noted that the nanosheets consist of the assembly of spherical nanoparticles after transformation from LDH to NCO. Also, an increase of pH from 8 to 13 during synthesis results in smaller particle sizes after annealing. As expected, the morphology of the NCO14 is transferred from NCO14B. Regardless of different pH, homogenous distribution of the constituent elements (Ni, Co, and O) was observed from NCOBs and NCOs as shown in Figure S2, which implies that the synthesis route using the chemical bath method is applicable to prepare the spinel-type $NiCo_2O_4$ nanostructures at comparatively low temperature (450 °C).

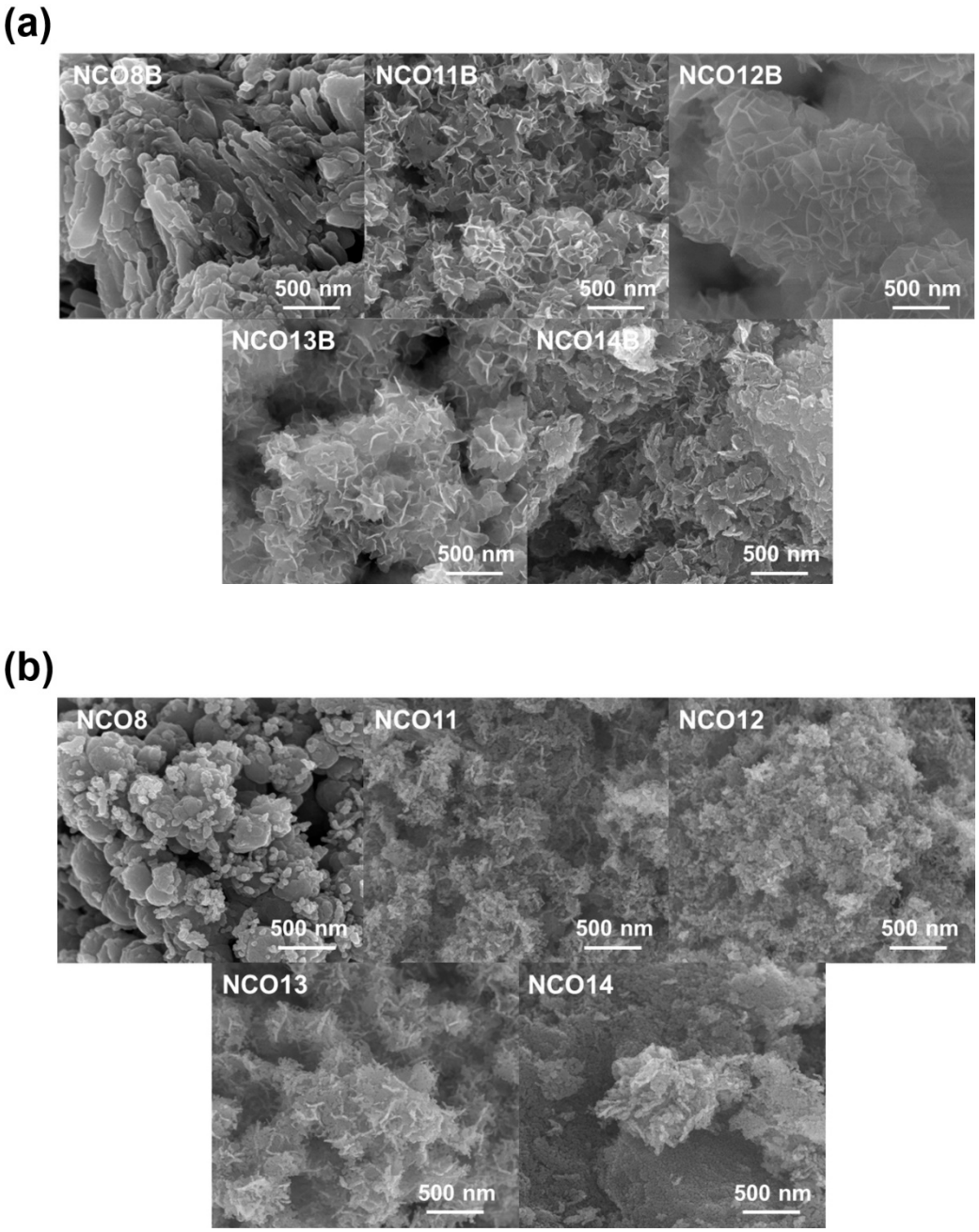

Figure 2. FE-SEM images of (**a**) NCOBs (8B, 11B, 12B, 13B, and 14B), and (**b**) NCOs (8, 11, 12, 13, and 14).

Different microstructures of the NCOs can be determined by different processing conditions including pH, thus showing different electrochemical properties. The dependence of the cyclic voltammetric (CV) curves for NCOs on the pH during chemical bath synthesis was measured to investigate the electrochemical behavior of the NCOs under alkaline conditions (0.1 M NaOH) at various scan rates as shown in Figure 3. There is a negligible effect of pH on the redox peak potentials for the NCO electrodes. Regardless of pH, redox peak currents of the NCOs were increased with increasing CV scan rate. Oxidation peaks of the NCOs correspond to Ni^{2+}/Ni^{3+}, Co^{2+}/Co^{3+}, and Co^{3+}/Co^{4+} due to oxidation of Ni^{2+}, Co^{2+} and Co^{3+} to Ni^{3+}, Co^{3+}, and Co^{4+}, respectively. It is noted that the redox peak potential of Co^{3+}/Co^{4+} is close to that of Ni^{2+}/Ni^{3+} and Co^{2+}/Co^{3+}, which shows overlapped redox peaks in the CV curve [35–37]. In addition, the reduction peaks of NCOs are attributed to the Ni^{3+}, Co^{4+}, and Co^{3+} to Ni^{2+}, Co^{3+}, and Co^{2+}, respectively. The redox peak currents for the NCOs at the square root of the scan rates are presented in

Figure 3f. All NCOs synthesized at different pH show a linear proportionality relationship between the redox peak currents and the square root of the scan rates, suggesting that NCOs undergo diffusion-controlled electrochemical behavior [38,39]. Also, CV responses of NCOs were synthesized at different pH in response to 5 mM glucose under alkaline conditions (0.1 M NaOH) at a scan rate of 50 mVs^{-1}, as shown in Figure S3. Regardless of the pH, all NCOs oxidize glucose ($C_6H_{12}O_6$) to gluconolactone ($C_6H_{10}O_6$), which implies that NCOs synthesized at different pH can be applied to electrochemical glucose sensors [40,41].

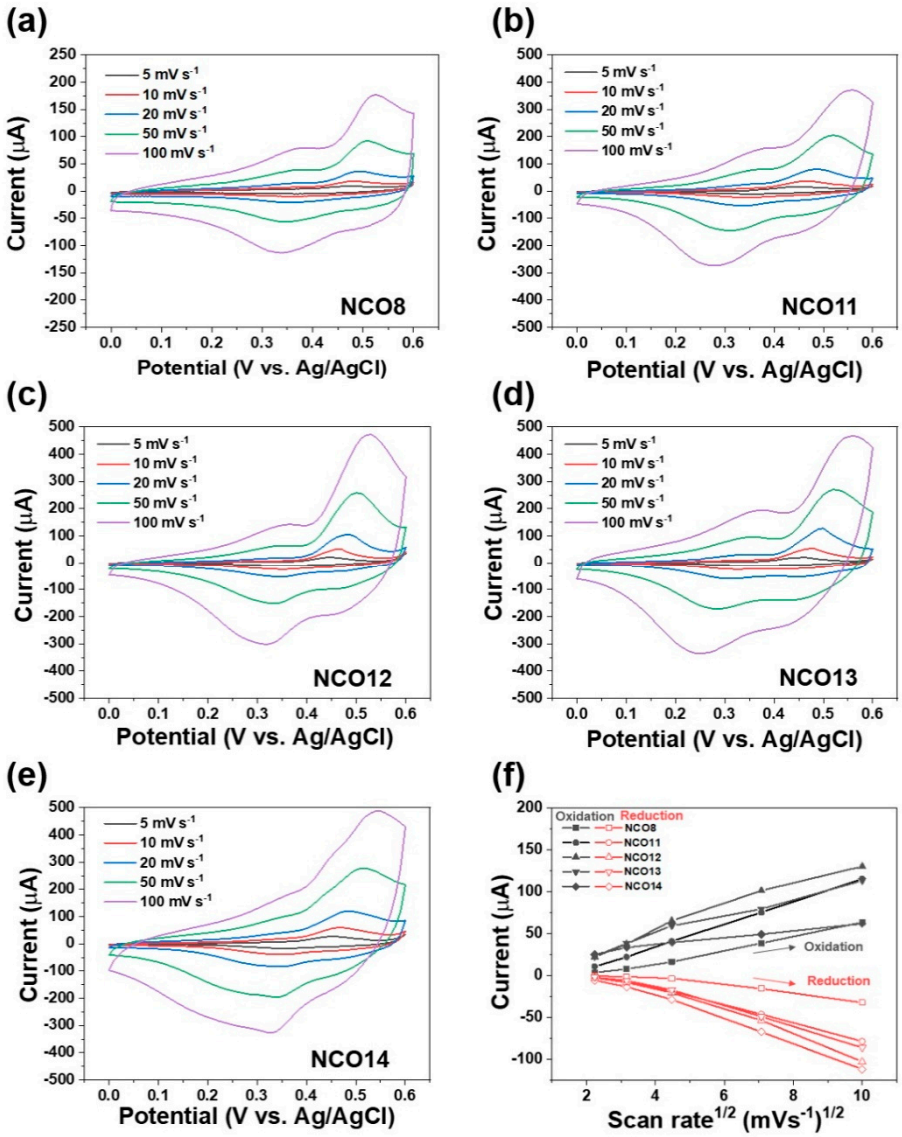

Figure 3. CV curves of (**a**) NCO8, (**b**) NCO11, (**c**) NCO12, (**d**) NCO13, and (**e**) NCO14 electrodes at different scan rates in 0.1 M NaOH solution. (**f**) Respective Randles–Sevcik plots of NCO electrodes.

The electrochemical performance of NCOs on glucose oxidation was investigated as shown in Figure 4. Chronoamperometry (CA) responses of NCOs were measured by stepwise changes in glucose concentrations in 0.1 M NaOH at 60 s intervals under an applied potential of 0.50 V. With increasing pH during synthesis, the sensitivity of NCO shows in the range between 48.71–146.26 μA/mM (cm^2) with 0.995–0.998 (R^2), which shows a linear detection limit in the range between 0.01–6 mM. The limits of detection (LOD) of NCOs are in the range between 0.0475–0.393 μM, as shown in Figure S4. Based on the results from the CA test, NCO13 shows superior electrochemical performance for

glucose detection, supported by excellent linear sensitivity (146.24 μA/mM (cm^2)) in a wide detection range. The excellent sensitivity of the NCOs is strongly associated with the redox reaction of active sites. As expected, Co^{2+}, Co^{3+}, Ni^{2+}, and Ni^{3+} as active sites in NCO were investigated in XPS results, as shown in Figure S5. In the XPS spectra of Co2p and Ni2p, $Co^{2+}/^{3+}$ and $Ni^{2+}/^{3+}$ were observed on the NCO. It is believed that multi-valence states of Ni and Co cations play an important role as oxidizing agents for glucose detection [17,42,43]. Thus, the reversible conversion of Ni^{2+}/Ni^{3+} and Co^{2+}/Co^{3+} in NCOs enables repetitive glucose detection [44–46].

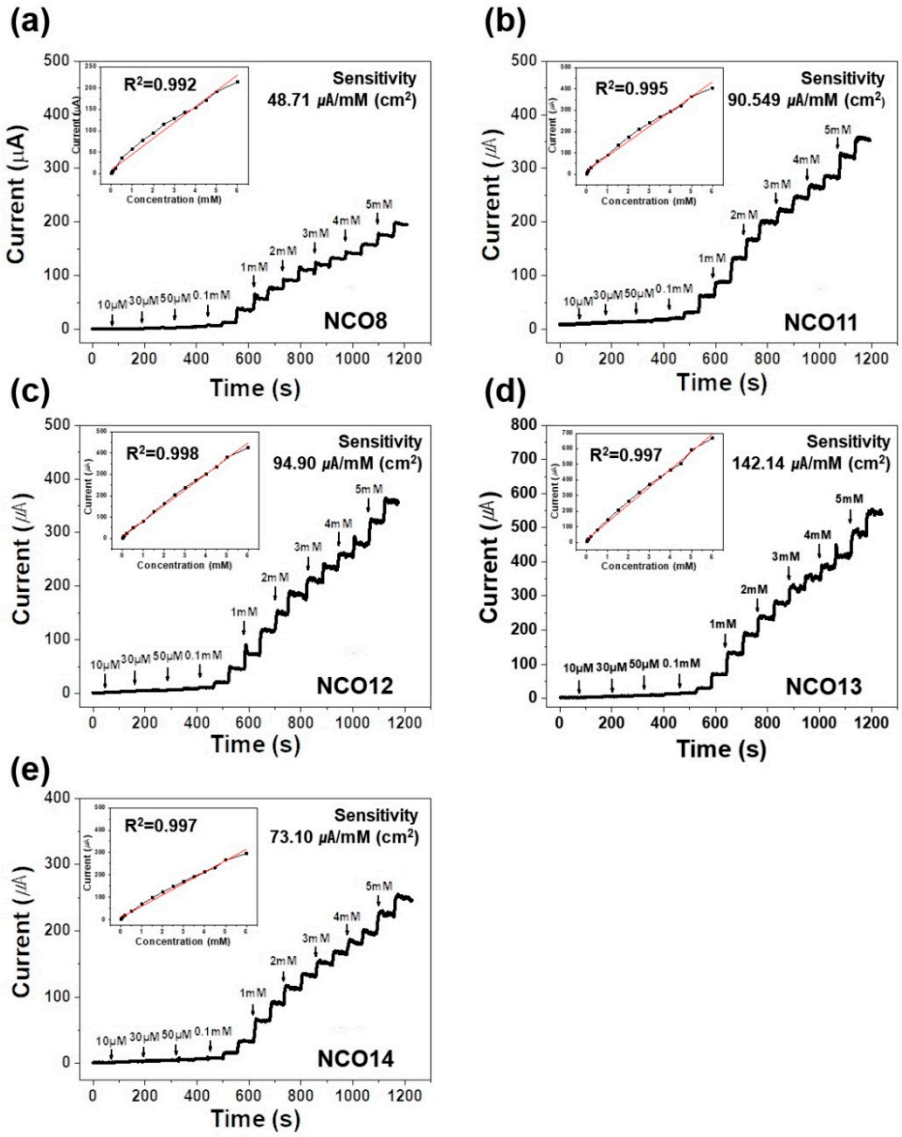

Figure 4. CA responses of (**a**) NCO8, (**b**) NCO11, (**c**) NCO12, (**d**) NCO13, and (**e**) NCO14 electrodes with the addition of glucose to 0.1 M NaOH solution at 0.50 V. Their respective calibration curves of current response versus glucose concentration plots inset in the figure.

The selectivity of NCOs is also an important factor for accurate glucose detection: current response to other reagents can detract from the determination of glucose [47–49]. The selectivity of the NCOs depending on different pH was investigated as shown in Figure 5. The current response of all NCOs to glucose is obvious. However, there is no change in the current response to uric acid (UA), dopamine (DA), L-ascorbic acid (LA), and acetic acid (AA) at the same glucose concentration of 1 and 2 mM, which implies that NCOs have excellent selectivity for glucose [41,50,51]. Based on the results above, it is

suggested that the sensitivity of the NCOs for glucose detection is strongly dependent on morphology, however, selectivity for glucose detection is significantly determined by the redox reaction of the chemical components. The electrochemical performance of the NCOs prepared in this work was summarized in Table 1. The sensitivity of the $NiCo_2O_4$/rGO shows the highest value when compared to the other materials including NCOs, induced by the excellent electrochemical performance of the NCOs combined with fast electron transfer from supportive rGO [52–55]. However, NCOs show higher sensitivity with a lower detection limit in response to glucose compared to the rest of the materials in Table 1 [56–58]. Therefore, the NCOs as pure oxides can be expected to be practical for the application of glucose sensors.

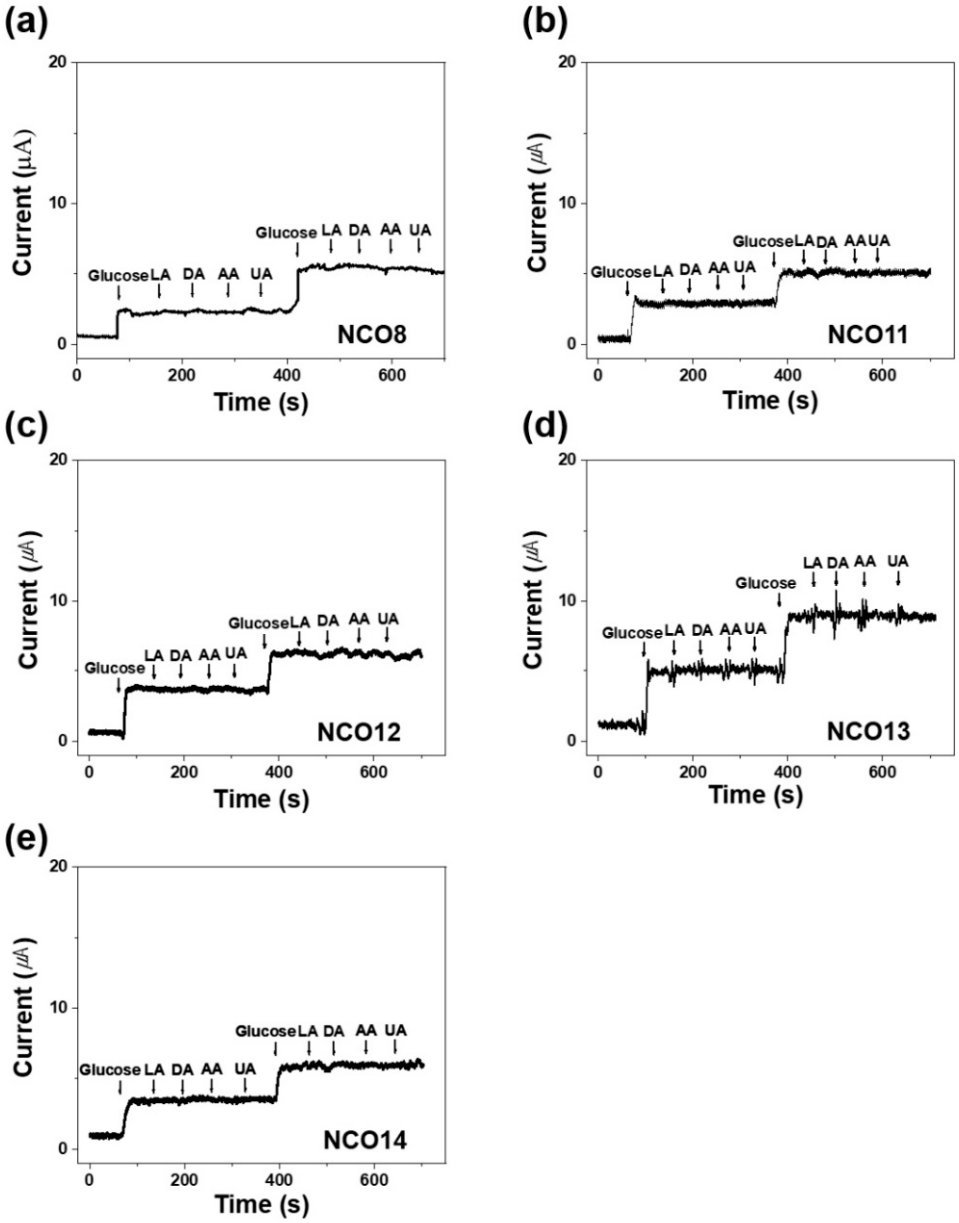

Figure 5. CA responses (CA) of (**a**) NCO8, (**b**) NCO11, (**c**) NCO12, (**d**) NCO13, and (**e**) NCO14 electrodes to addition of 1 mM glucose and 0.1 mM interfering species (LA, DA, AA, and UA) in a 0.1 M NaOH solution at 0.5 V.

Table 1. Comparison of our work to the nonenzymatic glucose sensor.

Electrode	Method	Sensitivity (μA/mM (cm^2))	Linear Range (mM)	Correlation Coefficient (R^2)	Detection Limit (μM)	Refs.
NCO8	CA	48.71	0.01–6	0.992	0.539	This work
NCO11	CA	90.549	0.01–6	0.995	0.393	This work
NCO12	CA	94.90	0.01–6	0.998	0.0503	This work
NCO13	CA	142.14	0.01–6	0.997	0.0433	This work
NCO14	CA	73.10	0.01–6	0.996	0.0475	This work
$NiCo_2O_4$/CNT	CA	66.15	0.02–12.12	0.99	5	[52]
$NiCo_2O_4$/rGO	CA	548.9	0.005–8.56	0.99	2	[53]
$CuCo_2O_4$	CA	3.625	Up to 0.32	-	5	[56]
NiO	CA	32.91	Up to 1.94		1.28	[57]
Co_3O_4	CA	36.25	Up to 2.04		0.97	[58]

4. Conclusions

Spinel-type $NiCo_2O_4$ (NCO) nanostructure was synthesized by a simple chemical bath method for electrochemical glucose sensors. Although different chemical reactions and formation of intermediates depending on pHs occur during synthesis, only spinel-type NCO was prepared after annealing at 450 °C. However, the morphology and particle size of the NCOs are strongly influenced by pH value, which emphasizes the importance of synthetic routes for the formation of the NCO. In our study, NCO13 with flower-like morphology assembled with small nanoparticles shows superior glucose detection including a sensitivity of 143 μA/mM (cm^2) up to 6 mM with good linearity. It is revealed that the different morphology and particle size of the NCO determine the sensitivity for glucose detection. Also, the selectivity of the NCO is determined by the unique spinel structure and redox reaction of Ni and Co ions.

Supplementary Materials: The following are available online at https://www.mdpi.com/2079-4991/11/1/55/s1, Figure S1: CA response of NCO13 electrode upon addition of 1 mM glucose in 1m M NaOH solution at different applied potentials. Figure S2: SEM-elemental mapping images of (a) NCOBs (8B, 11B, 12B, 13B, and 14B), and (b) NCOs (8, 11, 12, 13, and 14). Figure S3: CV curves of (a) NCO8, (b) NCO11, (c) NCO12, (d) NCO13, and (e) NCO14 electrodes in the absence of glucose and with 5 mM concentration of glucose at a scan rate 50 mVs^{-1}. Figure S4: CA response of (a) NCO8, (b) NCO11, (c) NCO12, (d) NCO13, and (e) NCO14 electrodes with the addition of 10 μM glucose in 0.1 M NaOH solution at 0.50 V. Figure S5: The XPS spectra of Ni2p and Co2p (NCO13). Table S1: Sample notations of As-prepared and after annealing samples.

Author Contributions: K.-b.J.: data curation, formal analysis, investigation, and writing-original draft. K.R.P.: data curation, formal analysis, investigation, and writing-original draft. K.M.K.: investigation, and methodology. S.-k.H.: data curation, and investigation. J.-e.J.: data curation, investigation, and methodology. Y.S.S.: data curation, and investigation. S.-k.P.: formal analysis, and funding acquisition. K.-i.M.: formal analysis, and funding acquisition. C.A.: data curation, investigation, and resources. S.-c.L.: formal analysis, and project administration. J.L.: investigation, and methodology. J.C.K.: writing-review and editing. H.H.: writing-review and editing. S.M.: conceptualization, formal analysis, writing-review and editing. All authors have read and agreed to the published version of the manuscript.

Funding: This study has been conducted with the support of the Korea Institute of Industrial Technology as "Development of intelligent root technology with add-on modules (kitech EO200017)". This work was supported by the National Research Foundation of Korea (NRF) grant funded by the Korea government (MSIT) (No. NRF-2020R1A2C1101466).

Institutional Review Board Statement: Not applicable.

Informed Consent Statement: Not applicable.

Conflicts of Interest: The authors declare no conflict of interest.

References

1. Cho, N.; Shaw, J.E.; Karuranga, S.; Huang, Y.; da Rocha Fernandes, J.D.; Ohlrogge, A.W.; Malanda, B. IDF Diabetes Atlas: Global estimates of diabetes prevalence for 2017 and projections for 2045. *Diabetes Res. Clin. Pract.* **2018**, *138*, 271–281. [CrossRef]
2. Song, S.O.; Song, Y.D.; Nam, J.Y.; Park, K.H.; Yoon, J.H.; Son, K.M.; Lim, D.H. Epidemiology of type 1 diabetes mellitus in Korea through an investigation of the national registration project of type 1 diabetes for the reimbursement of glucometer strips with additional analyses using claims data. *Diabetes. Metab. J.* **2016**, *40*, 35–45. [CrossRef]
3. Abellán-Llobregat, A.; Jeerapan, I.; Bandodkar, A.; Vidal, L.; Canals, A.; Wang, J.; Morallon, E. A stretchable and screen-printed electrochemical sensor for glucose determination in human perspiration. *Biosens. Bioelectron.* **2017**, *91*, 885–891. [CrossRef]
4. Ensafi, A.A.; Zandi-Atashbar, N.; Rezaei, B.; Ghiaci, M.; Taghizadeh, M. Silver nanoparticles decorated carboxylate functionalized SiO_2, new nanocomposites for non-enzymatic detection of glucose and hydrogen peroxide. *Electrochim. Acta.* **2016**, *214*, 208–216. [CrossRef]
5. Bandodkar, A.J.; Wang, J. Non-invasive wearable electrochemical sensors: A review. *Trends Biotechnol.* **2014**, *32*, 363–371. [CrossRef]
6. Yao, H.; Liao, Y.; Lingley, A.R.; Afanasiev, A.; Lähdesmäki, I.; Otis, B.P.; Parviz, B.A. A contact lens with integrated telecommunication circuit and sensors for wireless and continuous tear glucose monitoring. *J. Micromech. Microeng.* **2012**, *22*, 075007. [CrossRef]
7. Kim, D.M.; Moon, J.M.; Lee, W.C.; Yoon, J.H.; Choi, C.S.; Shim, Y.B. A potentiometric non-enzymatic glucose sensor using a molecularly imprinted layer bonded on a conducting polymer. *Biosens. Bioelectron.* **2017**, *91*, 276–283. [CrossRef] [PubMed]
8. Chung, J.S.; Hur, S.H. A highly sensitive enzyme-free glucose sensor based on Co_3O_4 nanoflowers and 3D graphene oxide hydrogel fabricated via hydrothermal synthesis. *Sens. Actuators B Chem.* **2016**, *223*, 76–82.
9. Wang, J. Glucose biosensors: 40 years of advances and challenges. *Electroanalysis.* **2013**, *13*, 983–988. [CrossRef]
10. Jia, W.Z.; Wang, K.; Zhu, Z.J.; Song, H.T.; Xia, X.H. One-step immobilization of glucose oxidase in a silica matrix on a Pt electrode by an electrochemically induced sol−gel process. *Langmuir* **2007**, *23*, 11896–11900. [CrossRef] [PubMed]
11. Bo, X.; Ndamanisha, J.C.; Bai, J.; Guo, L. Nonenzymatic amperometric sensor of hydrogen peroxide and glucose based on Pt nanoparticles/ordered mesoporous carbon nanocomposite. *Talanta.* **2010**, *82*, 85–91. [CrossRef]
12. Yuan, J.H.; Wang, K.; Xia, X.H. Highly ordered platinum-nanotubule arrays for amperometric glucose sensing. *Adv Funct Mater.* **2005**, *15*, 803–809. [CrossRef]
13. Martins, A.; Ferreira, V.; Queirós, A.; Aroso, I.; Silva, F.; Feliu, J. Enantiomeric electro-oxidation of d-and l-glucose on chiral gold single crystal surfaces. *Electrochem Commun.* **2003**, *5*, 741–746. [CrossRef]
14. Niu, X.; Lan, M.; Chen, C.; Zhao, H. Nonenzymatic electrochemical glucose sensor based on novel Pt–Pd nanoflakes. *Talanta.* **2012**, *99*, 1062–1067. [CrossRef]
15. Yuan, C.; Wu, H.B.; Xie, Y.; Lou, X.W. Mixed transition-metal oxides: Design, synthesis, and energy-related applications. *Angew. Chem. Int. Ed.* **2014**, *53*, 1488–1504. [CrossRef] [PubMed]
16. Wu, Z.; Zhu, Y.; Ji, X. $NiCo_2O_4$-based materials for electrochemical supercapacitors. *J. Mater. Chem. A* **2014**, *2*, 14759–14772. [CrossRef]
17. Naik, K.K.; Kumar, S.; Rout, C.S. Electrodeposited spinel $NiCo_2O_4$ nanosheet arrays for glucose sensing application. *RSC Adv.* **2015**, *5*, 74585–74591. [CrossRef]
18. Li, G.; Huo, H.; Xu, C. $Ni_{0.31}Co_{0.69}S_2$ nanoparticles uniformly anchored on a porous reduced graphene oxide framework for a high-performance non-enzymatic glucose sensor. *J. Mater. Chem. A* **2015**, *3*, 4922–4930. [CrossRef]
19. Marco, J.F.; Gancedo, J.R.; Gracia, M.; Gautier, J.L.; Rios, E.; Berry, F.J. Characterization of the nickel cobaltite, $NiCo_2O_4$, prepared by several methods: An XRD, XANES, EXAFS, and XPS study. *J. Solid State Chem.* **2000**, *153*, 74–81. [CrossRef]
20. Cabo, M.; Pellicer, E.; Rossinyol, E.; Estrader, M.; López-Ortega, A.; Nogués, J.; Baró, M.D. Synthesis of compositionally graded nanocast $NiO/NiCo_2O_4/Co_3O_4$ mesoporous composites with tunable magnetic properties. *J. Mater. Chem.* **2010**, *20*, 7021–7028. [CrossRef]
21. Wang, N.; Sun, B.; Zhao, P.; Yao, M.; Hu, W.; Komarneni, S. Electrodeposition preparation of $NiCo_2O_4$ mesoporous film on ultrafine nickel wire for flexible asymmetric supercapacitors. *Chem. Eng. J.* **2018**, *345*, 31–38. [CrossRef]
22. Zhang, J.; Sun, Y.; Li, X.; Xu, J. Fabrication of $NiCo_2O_4$ nanobelt by a chemical co-precipitation method for non-enzymatic glucose electrochemical sensor application. *J. Alloys Compd.* **2020**, 154796. [CrossRef]
23. Wang, J.; Zhang, Y.; Ye, J.; Wei, H.; Hao, J.; Mu, J.; Hussain, S. Facile synthesis of three-dimensional $NiCo_2O_4$ with different morphology for supercapacitors. *RSC Adv.* **2016**, *6*, 70077–70084. [CrossRef]
24. Chi, B.; Li, J.; Han, Y.; Chen, Y. Effect of temperature on the preparation and electrocatalytic properties of a spinel $NiCo_2O_4$/Ni electrode. *Int. J. Hydrog. Energy.* **2004**, *29*, 605–610. [CrossRef]
25. Guragain, D.; Zequine, C.; Poudel, T.; Neupane, D.; Gupta, R.K.; Mishra, S.R. Influence of Urea on the Synthesis of $NiCo_2O_4$ Nanostructure: Morphological and Electrochemical Studies. *J. Nanosci. Nanotechnol.* **2020**, *20*, 2526–2537. [CrossRef]
26. Cui, B.; Lin, H.; Li, J.B.; Li, X.; Yang, J.; Tao, J. Core–ring structured $NiCo_2O_4$ nanoplatelets: Synthesis, characterization, and electrocatalytic applications. *Adv. Funct. Mater.* **2008**, *18*, 1440–1447. [CrossRef]

27. Valdez, R.; Grotjahn, D.B.; Smith, D.K.; Quintana, J.M.; Olivas, A. Nanosheets of Co-(Ni and Fe) layered double hydroxides for electrocatalytic water oxidation reaction. *Int. J. Electrochem. Sci.* **2015**, *10*, 909–918.
28. Hu, L.; Wu, L.; Liao, M.; Fang, X. High-Performance $NiCo_2O_4$ Nanofilm Photodetectors Fabricated by an Interfacial Self-Assembly Strategy. *Adv. Mater.* **2011**, *23*, 1988–1992. [CrossRef]
29. Cai, L.; Li, Y.; Xiao, X.; Wang, Y. The electrochemical performances of $NiCo_2O_4$ nanoparticles synthesized by one-step solvothermal method. *Ionics (Kiel)* **2017**, *23*, 2457–2463. [CrossRef]
30. Chen, X.; Li, H.; Xu, J.; Jaber, F.; Musharavati, F.; Zalezhad, E.; Liu, J. Synthesis and Characterization of a $NiCo_2O_4$@$NiCo_2O_4$ Hierarchical Mesoporous Nanoflake Electrode for Supercapacitor Applications. *Nanomaterials.* **2020**, *10*, 1292. [CrossRef]
31. Uke, S.J.; Chaudhari, G.N.; Bodade, A.B.; Mardikar, S.P. Morphology dependant electrochemical performance of hydrothermally synthesized $NiCo_2O_4$ nanomorphs. *Mater. Sci. Technol.* **2020**, *3*, 289–298. [CrossRef]
32. Liu, Y.; Jiang, J.; Yuan, Y.; Jiang, Q.; Yan, C. Vertically Aligned $NiCo_2O_4$ Nanosheet-Encapsulated Carbon Fibers as a Self-Supported Electrode for Superior Li^+ Storage Performance. *Nanomaterials.* **2019**, *9*, 1336. [CrossRef]
33. Yan, T.; Li, R.; Li, Z. Nickel–cobalt layered double hydroxide ultrathin nanoflakes decorated on graphene sheets with a 3D nanonetwork structure as supercapacitive materials. *Mater. Res. Bull.* **2014**, *51*, 97–104. [CrossRef]
34. Song, Q.; Tang, Z.; Guo, H.; Chan, S.L.I. Structural characteristics of nickel hydroxide synthesized by a chemical precipitation route under different pH values. *J. Power Sources.* **2002**, *112*, 428–434. [CrossRef]
35. Guo, Q.; Zeng, W.; Liu, S.; Li, Y. In situ formation of Co_3O_4 hollow nanocubes on carbon cloth-supported $NiCo_2O_4$ nanowires and their enhanced performance in non-enzymatic glucose sensing. *Nanotechnology.* **2020**, *31*, 265501. [CrossRef]
36. Wang, J.; Qiu, T.; Chen, X.; Lu, Y.; Yang, W. Hierarchical hollow urchin-like $NiCo_2O_4$ nanomaterial as electrocatalyst for oxygen evolution reaction in alkaline medium. *Power Sources.* **2014**, *268*, 341–348. [CrossRef]
37. Yu, Z.; Li, H.; Zhang, X.; Liu, N.; Tan, W.; Zhang, X.; Zhang, L. Facile synthesis of $NiCo_2O_4$@Polyaniline core–shell nanocomposite for sensitive determination of glucose. *Biosens. Bioelectron.* **2016**, *75*, 161–165. [CrossRef]
38. Hassanpoor, S.; Aghely, F. Hierarchically self-assembled $NiCo_2O_4$ nanopins as a high-performance supercapacitor cathodic material: A morphology controlled study. *RSC Adv.* **2020**, *10*, 35235–35244. [CrossRef]
39. Zhan, J.; Cai, M.; Zhang, C.; Wang, C. Synthesis of mesoporous $NiCo_2O_4$ fibers and their electrocatalytic activity on direct oxidation of ethanol in alkaline media. *Electrochim. Acta.* **2015**, *154*, 70–76. [CrossRef]
40. Yu, H.; Jin, J.; Jian, X.; Wang, Y.; Qi, G.C. Preparation of cobalt oxide nanoclusters/overoxidized polypyrrole composite film modified electrode and its application in nonenzymatic glucose sensing. *Electroanalysis* **2013**, *25*, 1665–1674. [CrossRef]
41. Pasta, M.; La Mantia, F.; Cui, Y. Mechanism of glucose electrochemical oxidation on gold surface. *Electrochim. Acta.* **2010**, *55*, 5561–5568. [CrossRef]
42. Saraf, M.; Natarajan, K.; Mobin, S.M. Multifunctional porous $NiCo_2O_4$ nanorods: Sensitive enzymeless glucose detection and supercapacitor properties with impedance spectroscopic investigations. *New J. Chem.* **2017**, *41*, 9299–9313. [CrossRef]
43. Amin, B.G.; Masud, J.; Nath, M. A non-enzymatic glucose sensor based on a $CoNi_2Se_4$/rGO nanocomposite with ultrahigh sensitivity at low working potential. *J. Mater. Chem. B.* **2019**, *7*, 2338–2348. [CrossRef]
44. Li, H.; Zhang, L.; Mao, Y.; Wen, C.; Zhao, P. A simple electrochemical route to access amorphous Co-Ni hydroxide for non-enzymatic glucose sensing. *Nanoscale Res. Lett.* **2019**, *14*, 1–12. [CrossRef]
45. Cui, S.; Zhang, J.; Ding, Y.; Gu, S.; Hu, P.; Hu, Z. Rectangular flake-like mesoporous $NiCo_2O_4$ as enzyme mimic for glucose biosensing and biofuel cell. *Sci. China Mater.* **2017**, *60*, 766–776. [CrossRef]
46. Huang, W.; Cao, Y.; Chen, Y.; Peng, J.; Lai, X.; Tu, J. Fast synthesis of porous $NiCo_2O_4$ hollow nanospheres for a high-sensitivity non-enzymatic glucose sensor. *Appl. Surf. Sci.* **2017**, *396*, 804–811. [CrossRef]
47. Wang, C.; Du, J.; Wang, H.; Zou, C.E.; Jiang, F.; Yang, P.; Du, Y. A facile electrochemical sensor based on reduced graphene oxide and Au nanoplates modified glassy carbon electrode for simultaneous detection of ascorbic acid, dopamine and uric acid. *Sens. Actuators B Chem.* **2014**, *204*, 302–309. [CrossRef]
48. Jiménez-Fiérrez, F.; González-Sánchez, M.I.; Jiménez-Pérez, R.; Iniesta, J.; Valero, E. Glucose Biosensor Based on Disposable Activated Carbon Electrodes Modified with Platinum Nanoparticles Electrodeposited on Poly (Azure A). *Sensors.* **2020**, *20*, 4489. [CrossRef]
49. Gong, X.; Gu, Y.; Zhang, F.; Liu, Z.; Li, Y.; Chen, G.; Wang, B. High-performance non-enzymatic glucose sensors based on CoNiCu alloy nanotubes arrays prepared by electrodeposition. *Front. Mater.* **2019**, *6*, 3. [CrossRef]
50. Mondal, S.; Madhuri, R.; Sharma, P.K. Probing the shape-specific electrochemical properties of cobalt oxide nanostructures for their application as selective and sensitive non-enzymatic glucose sensors. *J. Mater. Chem. C.* **2017**, *5*, 6497–6505. [CrossRef]
51. Ding, Y.; Wang, Y.; Su, L.; Bellagamba, M.; Zhang, H.; Lei, Y. Electrospun Co_3O_4 nanofibers for sensitive and selective glucose detection. *Biosens. Bioelectron.* **2010**, *26*, 542–548. [CrossRef] [PubMed]
52. Wang, L.; Lu, X.; Ye, Y.; Sun, L.; Song, Y. Nickel-cobalt nanostructures coated reduced graphene oxide nanocomposite electrode for nonenzymatic glucose biosensing. *Electrochim. Acta.* **2016**, *114*, 484–493. [CrossRef]
53. Ma, G.; Yang, M.; Li, C.; Tan, H.; Deng, L.; Xie, S.; Song, Y. Preparation of spinel nickel-cobalt oxide nanowrinkles/reduced graphene oxide hybrid for nonenzymatic glucose detection at physiological level. *Electrochim. Acta.* **2016**, *220*, 545–553. [CrossRef]
54. Liu, Y.; Liu, X.; Guo, Z.; Hu, Z.; Xue, Z.; Lu, X. Horseradish peroxidase supported on porous graphene as a novel sensing platform for detection of hydrogen peroxide in living cells sensitively. *Biosens. Bioelectron.* **2017**, *87*, 101–107. [CrossRef]

55. Zhang, C.; Zhang, Y.; Du, X.; Chen, Y.; Dong, W.; Han, B.; Chen, Q. Facile fabrication of Pt-Ag bimetallic nanoparticles decorated reduced graphene oxide for highly sensitive non-enzymatic hydrogen peroxide sensing. *Talanta* **2016**, *159*, 280–286. [CrossRef]
56. Kannan, P.K.; Hu, C.; Morgan, H.; Rout, C.S. One-Step Electrodeposition of $NiCo_2S_4$ Nanosheets on Patterned Platinum Electrodes for Non-Enzymatic Glucose Sensing. *Chem. Asian. J.* **2016**, *11*, 1837–1841. [CrossRef]
57. Liu, S.; Hui, K.S.; Hui, K.N. Flower-like copper cobaltite nanosheets on graphite paper as high-performance supercapacitor electrodes and enzymeless glucose sensors. *ACS Appl. Mater. Interfaces.* **2016**, *8*, 3258–3267. [CrossRef]
58. Ding, Y.; Wang, Y.; Zhang, L.; Zhang, H.; Lei, Y. Preparation, characterization and application of novel conductive NiO–CdO nanofibers with dislocation feature. *J. Mater. Chem.* **2012**, *22*, 980–986. [CrossRef]